05,09

Magneto-optical properties of nanoparticle dispersions based on Fe_3O_4, obtained by pulse laser ablation in a liquid

© O.V. Solodova[1], A.E. Sokolov[1,2], O.S. Ivanova[1,2,¶], M.N. Volochaev[1,3], I.N. Lapin[4], D.A. Goncharova[4], V.A. Svetlichnyi[4]

[1] Kirensky Institute of Physics, Federal Research Center KSC SB, Russian Academy of Sciences, Krasnoyarsk, Russia
[2] Siberian Federal University, Krasnoyarsk, Russia
[3] Immanuel Kant Baltic Federal University, Kaliningrad, Russia
[4] Tomsk State University, Tomsk, Russia
[¶] E-mail: osi@iph.krasn.ru

Received June 16, 2021
Revised June 24, 2021
Accepted June 25, 2021

The structure, optical and magneto-optical properties of colloidal solutions of iron oxide nanoparticles obtained by pulsed ablation in distilled water, both without additives and with various functional additives: gold-hydrochloric acid, silicon oxide, and polyvinylpyrrolidone, have been studied. It is shown that the main magnetic phase is magnetite Fe_3O_4. The size distribution of nanoparticles and the degree of their agglomeration depend on the additives. In the absence of the latter, a very wide of size distributions and strong agglomeration of particles are observed. The narrowest distribution curve with a maximum corresponding to ~ 7 nm and an almost complete absence of agglomeration are observed for particles synthesized in the presence of polyvinylpyrrolidone. The shape of the spectral dependence of magnetic circular dichroism, which generally corresponds to the spectrum of magnetite, undergoes some modifications for various additives, which is associated with defects in the distribution of iron ions between different positions in the crystal.

Keywords: pulsed laser ablation, nanoparticles, colloidal solutions, magnetite, magnetic circular dichroism.

DOI: 10.21883/PSS.2022.14.54331.147

1. Introduction

Magnetic fluids based on colloidal solutions of nanoparticles (NPs) are of great interest from the point of view of application in modern industrial and medical technologies. The ability to change physical and chemical properties, up to the state of aggregation (liquid/solid) under the influence of a magnetic field, allows the use of magnetic fluids in a wide variety of applications [1,2]. The ability of oriented and structured magnetic fluids to change absorption in a wide range of the spectrum is of great interest, which is used to control the parameters of electromagnetic radiation in the THz area of the spectrum [3–6]. Another very wide and promising area of application of magnetic fluids is medicine, where such materials are used for magnetic separation, magnetic hyperthermia, magnetic targeted drug delivery [7], magnetic resonance imaging and a number of other applications [8–10]. The prospect of using magnetic fluids with NPs is due to the small size of the particles, high penetrating power, and the opportunity of remote handling with the help of a magnetic field.

One of the promising ways to obtain magnetic NPs immediately in the form of a colloidal solution is pulsed laser ablation (PLA) in a liquid [11,12]. Previously, the authors studied the properties of Fe_3O_4 magnetite NPs with an average size of ~ 10 nm, obtained by the PLA technique of a bulk metal target in distilled water, without introducing additional chemical precursors [12–14]. Colloidal solutions of such nanoparticles are unstable due to the aggregative instability of nanoparticles, which is associated with a small value of the zeta potential (~ 24 mV) and the position of the zero charge point 7.5 near the solution pH — 5.8 [12]. The presence of a magnetic moment also reduces stability by initiating aggregation and precipitation of particles. Therefore, such NPs, as a rule, require surface stabilization, which prevents them from sticking together and imparting certain functional properties to the surface [15–17]. Functionalization of the NP surface may be required, for example, for further attachment of active biological molecules (DNA aptamers, etc.) to them, to impart bio-inertness, reduce toxicity, or other properties important in each specific task, such as, for example, an albumin coating supports the function endothelium after intravenous administration of iron oxide nanoparticles to rats [18].

The significant dependence of the physical and chemical properties of colloidal solutions of NPs on the technique of their preparation, the state of the surface and the nature

of the solution dictates the need to conduct studies on the applicability of various colloidal solutions for solving a specific biomedical problem. Since the magnetic properties of a medium with magnetic NPs are determined as the properties of individual particles, and the effects of interaction between them, it is important to know the magnetic properties of the particles in the state in which they are supposed to be applied.

One of the effective tools for studying the phase composition and magnetic state of NPs are magnetooptical effects. Magnetic circular dichroism (MCD) is the most informative and convenient method for measuring of all the magnetooptical effects, since it is observed only in the absorption area and, as a rule, there is no contribution from the non-magnetic component of the medium [19]. MCD spectroscopy has a higher spectral resolution compared to optical spectroscopy; it was used by a number of authors to study NPs of iron oxides [20,21], not only to determine the magnitude of the magnetooptical response, but also as a tool, sometimes a key one, for identification of the NP phase composition, since the spectral dependence of this effect for different phases of iron oxide — magnetite (Fe_3O_4), maghemite (γ-Fe_2O_3) and hematite (α-Fe_2O_3) is unique and serves as an indisputable passport of these phases [22]. Let us note that obtaining a pure phase of any of the iron oxides is a very complex technological task, since insignificant thermal effects can lead to structural transformations in the chain of phases — magnetite, maghemite, epsilon phase and hematite: $Fe_3O_4 \rightarrow \gamma$-$Fe_2O_3 \rightarrow \varepsilon$-$Fe_2O_3 \rightarrow \alpha$-$Fe_2O_3$ [23,24]. In view of chemistry, magnetite is a metastable state with a reverse spinel structure $(Fe^{3+})[Fe^{3+}Fe^{2+}]O_4$ (parentheses denote tetrahedral, and square octahedral positions of iron ions) and the potential oxidation of Fe^{2+} ions due to the formation of vacancies in the lattice can transform it into maghemite $(Fe^{3+})[Fe^{3+}_{5/3}\square_{1/3}]O_4$, where $\square$ is a vacancy in the lattice. Maghemite, as well as subsequent iron oxides, contain only trivalent iron ions. Thus, in the work [25] the authors studied the transformation of a metastable magnetite phase into maghemite using the spectral dependences of the MCD. Since different iron oxide polymorphs have different magnetic properties and temperature changes in magnetic properties, for specific applications, it is required to accurately determine the NP phase composition. In a number of works, the structural and magnetic properties of all known forms of ferric oxides are excellently reviewed, as well as methods for their preparation with a discussion of the mechanisms leading to their formation, for example [26,27].

The aim of this work is to study the structure, phase composition, optical and magnetooptical properties of colloidal solutions of nanoparticles based on iron oxides, obtained by PLA in an aqueous medium with functional additives, in comparison with the properties of NPs obtained in distilled water.

2. Experimental part

2.1. Obtaining colloidal solutions of nanoparticles

Colloidal solutions of NPs were obtained by PLA in a liquid by irradiating the target with the fundamental harmonic of Nd : YAG laser LS2131M-20 (1064 nm, 180 mJ, 7 ns, 20 Hz). The target material was a plate of unalloyed low-carbon steel St.1kp (foreign analogue S185) with a purity of 99.5% and dimensions of $10 \times 40 \times 4$ mm. The experimental unit and conditions for obtaining nanocolloids are described in our previous studies [12,13].

PLA was carried out in distilled water without additives (hereinafter referred to as Fe-W) and with functional additives of various types. The concentration of NPs obtained by PLA was assessed by determining the mass loss of the target and amounted to 200 mg/l (by weight of metallic iron) for all samples. Gold-hydrochloric acid ($HAuCl_4 \cdot nH_2O$), Fe-W-Au sample; silicon dioxide, Fe-W-Si sample; polyvinylpyrrolidone (PVP) of 35,000 molecular weight, Fe-W-PVP sample were applied for functionalization.

Gold was thermally reduced on the NP surface and on the target surface in the ablation area during ablation in gold-hydrochloric acid. As a result, a dispersion was obtained with composite particles in the Fe : Au ratio equal to 10 : 1. Ablation of single-crystal silicon in water was preliminarily carried out (the PLA method for silicon in water, the characteristics of the obtained particles are given in [28]) to obtain a dispersion of particles functionalized with silicon oxide. As a result, a colloidal solution of predominantly X-ray amorphous silicon dioxide was obtained, after which the iron target was ablated in this dispersion. In the final dispersion, the Fe : Si ratio was 2 : 1. PLA of Fe was carried out in a preliminarily prepared PVP solution with a concentration of 0.5 wt.% to obtain a dispersion stabilized by a polymeric surfactant. The concentration of NPs in solutions in all cases was close and amounted to 200 mg/l.

2.2. Characterization of nanoparticles and dispersions

The morphology of the obtained NPs was studied using the transmission electron microscopy (TEM) technique using a Philips CM12 microscope with an accelerating voltage of 120 kV. A freshly made NP dispersion was deposited on a copper grid coated with a carbon film and dried at room temperature to carry out microscopic studies.

The crystal structure of the resulting material was studied by X-ray diffraction of the NP powder obtained by drying the dispersion on an XRD 6000 Shimadzu diffractometer (CuK_α-radiation with a wavelength of 1.54056 Å, scan angle range was $10-70^\circ$, scan step — 0.02°). The phase composition was identified using the PDF4 database. The distribution of the percentage of crystalline phases in the samples was assessed using the Powder Cell 2.4 software package. To minimize the effect of drying on the NP

structure, freshly made dispersions were dried in a vacuum chamber at room temperature.

The absorption spectra of nanocolloids were studied in a quartz cell using a Cary 100, Varian spectrophotometer in the wavelength range 200−900 nm.

Magnetooptical measurements were carried out in the range 1.6−3.9 eV (320−780 nm) on a laboratory unit for spectropolarimetric studies based on an MDR-2 monochromator. For measurements, acousto-optic modulation of the polarization mode of the light wave from right to left circular polarization was applied. The modulator electrode is a fused-silica prism with a piezoelectric ceramic element glued to it. An alternating electrical signal of frequency ω corresponding to the frequency of natural oscillations of the system is applied to the piezoelectric ceramic element, which leads to the formation of a standing wave in the quartz prism. In the lack of sound excitation, the prism is optically isotropic. When a half-wave of compression passes through it, the direction of propagation of sound excitation (along the horizontal axis of the prism) becomes the „slow" axis of the prism. When passing through the second half-wave (half-wave of extension), the picture becomes the opposite: the extension axis becomes the „fast" axis of the prism. If linear-polarized light is incident on a prism with the plane of polarization rotated through an angle of 45° with respect to the horizontal axis of the prism, then when a standing acoustic wave is generated in it, the light will be polarized in a circle at the output, and alternately on the right, then on the left with the frequency of acoustic oscillations of the prism. In the presence of the MCD effect in the sample under study, there is a difference between the absorption coefficients of light waves polarized in the right and left circles relative to the direction of the magnetic moment of the sample. Due to this, the light flux passing through the sample and then incident on the photomultiplier (PMT) turns out to be modulated in intensity and, accordingly, the variable signal at the output of the PMT will be proportional to the MCD value. The MCD value is determined as $\Delta D/D = (D_+ - D_-)/2(D_+ + D_-)$, where D_+ and D_- optical density of the medium are for light waves at two opposite directions of the external magnetic field, respectively. The principle of operation of the unit is described in detail in [29,30]. The spectral dependence of the MCD was measured discretely at fixed wavelengths in the selected spectral area. To determine the field dependence of the MCD, the sample was placed in a magnetic field with a variable strength and sign. The measurements were carried out at a wavelength of 495 nm (~ 2.5 eV), preliminarily determined from the spectral dependence of the MCD, there was absorption caused by the MCD for all samples. The field dependences of the MCD are proportional to the field dependence of the retained magnetization, which allowed to qualitatively assess the dependence of the sample magnetization on the external magnetic field. For measurements, colloidal solutions of samples were placed in transparent Baly tubes with an optical path length of 1 mm.

3. Results and discussion

3.1. Composition and structure of nanoparticles

Figure 1 shows TEM images of the synthesized NPs. The morphology and size characteristics of particles obtained by PLA in distilled water were studied in detail in [12,14]. The main fraction of particles is in the size range up to 10 nm, but there are some large spherical particles up to 80 nm in size and a large number of small particles with sizes of approximately 2 nm. The particle size distribution histograms obtained by processing the TEM image (Fig. 2) confirm this. It should be noted that small particles (up to 2 nm) due to the difficulty of their clear delineation were not included in the statistical processing, but a sufficient amount of them is present in the Fe-W sample. A peculiarity of this sample is that, due to the absence of stabilizing agents, NPs are assembled into rather dense agglomerates (Fig. 1, *a*), the size of which reaches several μm.

The application of high polymeric PVP (polymeric surfactant) in PLA as a stabilizer prevents the aggregation of NPs (Fig. 1, *b*), in this case, there is the narrowest particle size distribution, the main fraction of the particles is also in the size range up to 10 nm, with a distribution maximum of approximately 7 nm (Fig. 2, *b*). Ablation in water with the addition of gold-hydrochloric acid leads to the same effect — dispersion becomes stable, NPs do not agglomerate, and their size practically does not change (Fig. 1, *d*) and is in the range from 7 to 15 nm. A TEM image of a sample obtained by PLA of iron in a dispersion of silicon dioxide NPs is shown in Fig. 1, *c*. Due to close size characteristics and contrast, it is rather difficult to distinguish iron oxide nanoparticles against the background of silicon oxide. It can be noted that iron-containing particles are also mainly represented by a fraction up to 10 nm, separated by amorphous silicon dioxide, which forms various space configurations, including feather structures, and there are large particles of various sizes (Fig. 2, *c*).

Studies of the NP crystal structure obtained by PLA in water with and without precursors showed that, as a result of ablation, iron is in the oxide state in all samples, the absence of a reflection at 45°, which is the most intense reflection of metallic iron (Pdf Card № 01-071-4684), confirms this fact (Fig. 3). The signal in this area at the noise level allows to state that the volume concentration of this phase does not exceed 1% in the samples. The vertical dashed lines shown in Fig. 3 at $\sim$ 18, 30, 37, 42 53, 57 and 63° demonstrate the position of the characteristic peaks of magnetite Fe_3O_4 (Pdf Card № 04-002-3668), the coincidence of the reflections in the samples with their positions allows us to state that the iron in the samples is represented by cubic Fe_3O_4, point symmetry group Fd-3m. It is worthwhile noting that, as mentioned in the introduction, two polymorphic phases of iron oxide (magnetite and maghemite) have almost the same structure, and the X-ray diffraction curves do not give an unambiguous answer, especially in the case of weak insufficiently narrow

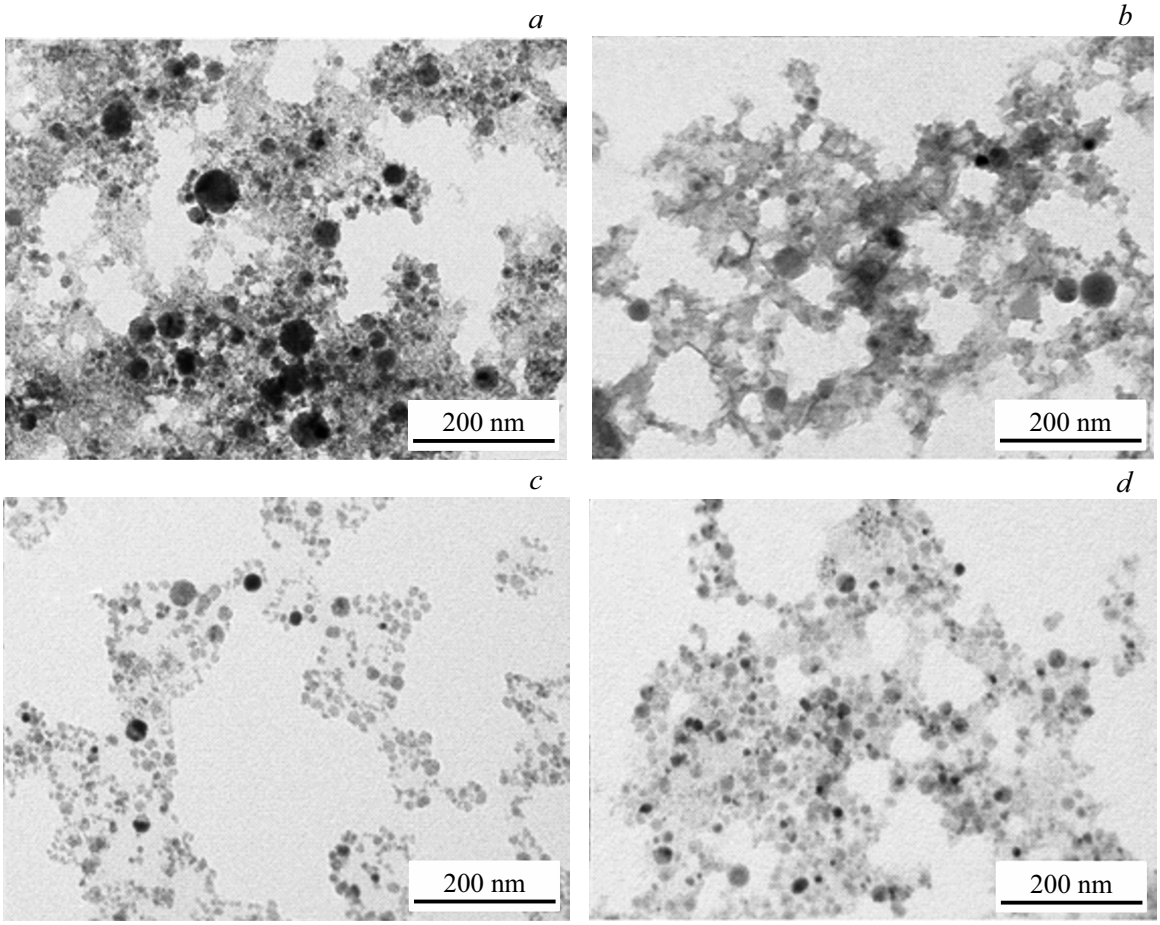

Figure 1. TEM images of NPs from colloidal solutions: Fe-W (a), Fe-W-PVP (b), Fe-W-Si (c) and Fe-W-Au (d).

reflections. Therefore, for accurate identification, it is desirable to resort to additional verification, for example, by studying the spectral dependence of the MCD, as was done in [22,25], and will be done below for the studied NPs. There are clearest reflections for the Fe-W-PVP and Fe-W-Au samples, which indicates a good NP crystallinity and a narrow size distribution in these samples, which is consistent with the TEM data (Fig. 1, b, d). The iron oxide reflections are the least expressed for the Fe-W-Si sample. This may be due to partial signal scattering on an amorphous silicon dioxide film covering Fe_3O_4 particles (Fig. 1, c). The broad reflections also testify to a large scatter in size. In the area of angles $15-30^\circ$ there is a wide band, presumably due to the contribution of the X-ray amorphous component of small iron clusters, which is most intense for the sample without Fe-W modifiers. For the Fe-W-PVP sample, the X-ray diffraction pattern in the area of angles $15-30^\circ$ additionally shows the contribution of the polymer component. In the Fe-W-Au sample, there are intense reflections of metallic gold of the cubic crystal system of the Fm-3m symmetry point group, formed during the reduction of gold-hydrochloric acid in the process of PLA. The presence of such intense reflections may indicate the formation of individual crystalline gold particles. Meanwhile, the results obtained do not allow us to unambiguously reject the formation of an even gold layer covering iron oxide NPs.

3.2. Absorption spectra of colloidal solutions

Absorption spectra of the NPs under study are presented in Fig. 4. The spectra of all samples are similar to each other, they do not contain expressed absorption peaks in the studied area and are characterized by a monotonic increase in absorbance in the UV area. An exception is the Fe-W-Au sample, for which there is an additional band in the area of $500-600$ nm, which is related to the surface plasmon resonance of gold nanostructures formed during the reduction of gold from gold-hydrochloric acid in the PLA process, which is confirmed by X-ray diffraction analysis data. Many authors, for example [21], have also observed a resonant absorption peak in this area in isolated gold particles, and it has been proven that it is due to surface plasmon resonance. For the Fe-W-Si sample, there is more intense absorption in the area shorter than 350 nm, probably due to the contribution of silicon dioxide particles. The absorption of PVP in the Fe-W-PVP sample does not appear

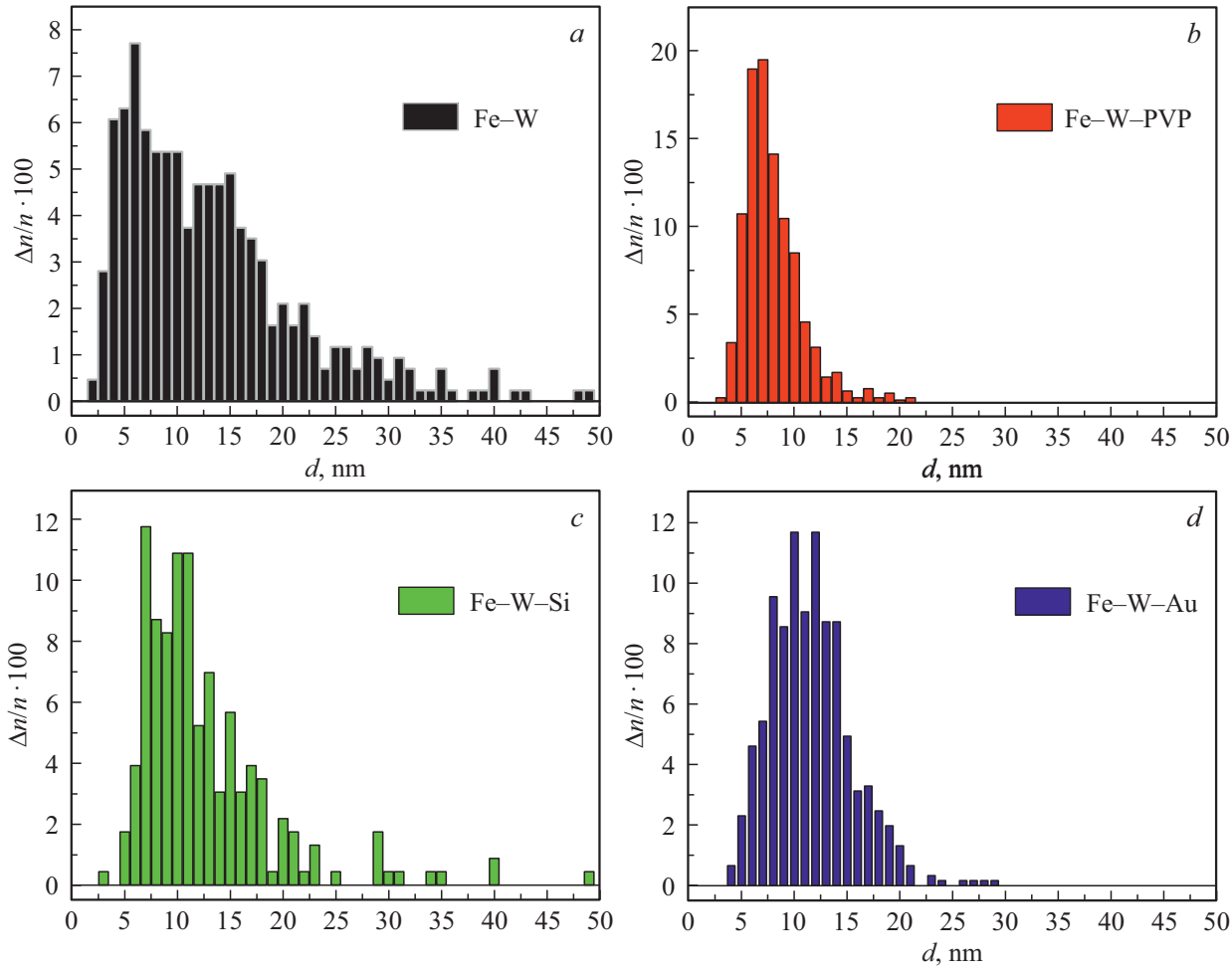

Figure 2. NP size distribution histograms obtained by processing TEM images of the samples: Fe-W (*a*), Fe-W-PVP (*b*), Fe-W-Si (*c*) and Fe-W-Au (*d*). The analysis was carried out with the use of Image J software.

in the spectrum, since it lies in the shorter wavelength area. In the spectra of all samples, there is a weakly expressed „shoulder" in the $\sim 300-340$ nm area. Its nature is discussed in the literature and can be associated both with metallic iron Fe(0) (α-Fe) [31], and with carbon — the formation of Fe_3C carbides from amorphous carbon on the particle surface [32].

3.3. Spectral dependences of MCD

In contrast to absorption spectra, MCD spectra (Fig. 5, *a*) demonstrate a rather complex structure, the prevailing components of which are two broad maxima of opposite signs. A similar character of the MCD spectrum, as well as the spectrum of the imaginary part of the off-diagonal component of the permittivity tensor, was observed in [20] for Fe_3O_4 nanoparticles dispersed in a film In_2O_3, as well as in [33] for Fe_3O_4 nanoparticles in a silicone matrix, and in [20,22,34,35] for Fe_3O_4 thin films. The similarity of the observed spectra with the results of the cited works suggests that the main contribution to the MCD in all the studied samples is associated with magnetite. No peculiarities were found in the MCD spectra characteristic of isomorphic magnetite, iron oxide γ-Fe_2O_3 [22], i.e. the identification of the nature of magnetic NPs based on the analysis of X-ray diffraction is unambiguous. However, the positions of the peculiarities in the spectra differ noticeably for different samples and, accordingly, in most cases differ from those in the MCD spectra presented in the literature. The spectrum for a colloidal solution of nanoparticles with silicon almost completely coincides with the literature data. In the case of the Fe-W sample, the entire spectrum is shifted to low energies and the high-energy peak is strongly broadened, while for the Fe-W-Au and Fe-W-PVP samples, both peaks obviously represent a superposition of at least two peaks. In order to understand how these peculiarities are related to the structure and composition of nanoparticles, let us consider what electronic excitations the peculiarities in the MCD spectrum can be associated with. Let us note that a comparison of the spectra of the samples in terms of signal intensity would be incorrect, since the concentration of NPs in solutions could change significantly over time due to a number of objective reasons: precipitation of large

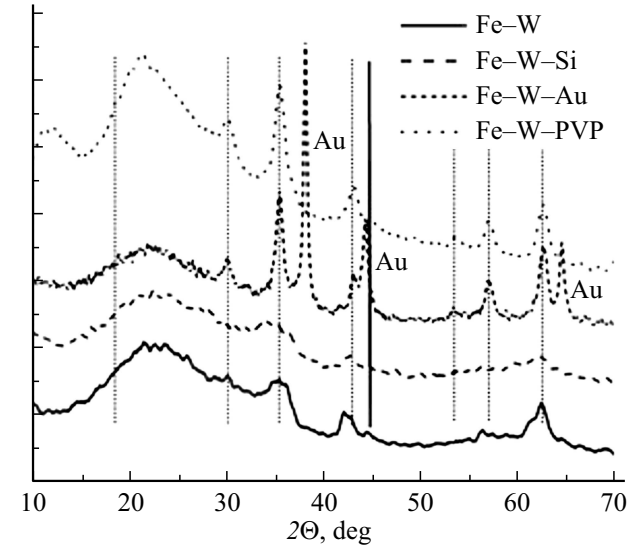

Figure 3. Diffraction patterns for powders from dispersions obtained by PLA of iron in water with and without functional additives. Solid vertical line at 45° — position of the most intense metallic iron reflection (Pdf Card № 01-071-4684), dashed lines at ∼ 18, 30, 37, 42, 53, 57 and 63° — position of characteristic peaks of magnetite Fe_3O_4 (Pdf Card № 04-002-3668), metallic gold peaks at 38, 44 and 64.5° are marked as Au (Pdf Card № 01-089-3697).

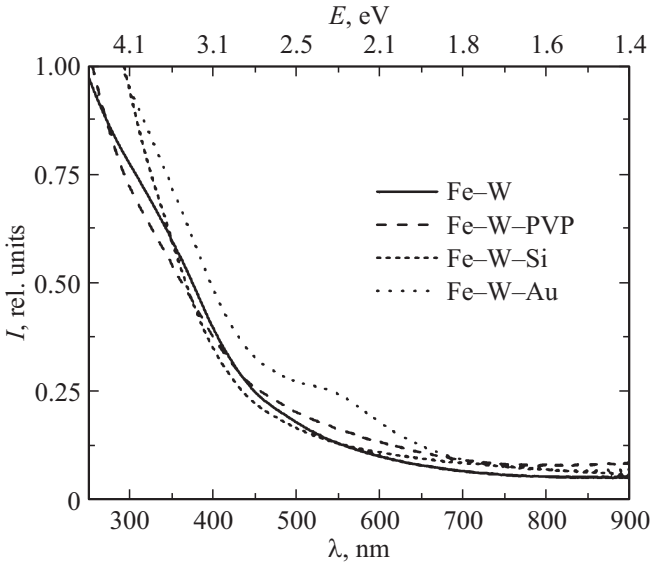

Figure 4. Absorption spectra of colloidal solutions obtained by PLA of iron in water with and without functional additives.

particles, agglomeration, etc. The spectrum of the Fe-W sample confirms this assumption, there is a weak signal with significant noise for this sample, there was a presence of a large spread of particles in size and a significant number of small agglomerations in this sample on TEM images (Fig. 1, *a*). In this regard, an analysis will be carried out for the shape and position of peculiarities in the MCD spectra. In addition, a very small number of studies of MCD in magnetite, carried out exclusively for the case of NPs, should be noted. Therefore, to compare the characteristics of the obtained MCD spectra with the literature data, the results of various authors on the study of the Kerr effect will be used, the spectral dependence of which is similar to the spectral dependence of the MCD.

As mentioned in the introduction, magnetite has a inverse spinel structure $(Fe^{3+})_A[Fe^{3+}Fe^{2+}]_B(O^{2-})_4$. Tetrahedral A-positions are occupied by Fe^{3+} ions, while octahedral B-positions are occupied equally by Fe^{3+} and Fe^{2+} ions. Fe^{2+} ions contain one „extra“ electron compared to Fe^{3+} ions. Since all B-positions are equivalent, at sufficiently high temperatures there are constant electron hops between ions, and it is currently accepted to consider the valency of iron ions in B-positions to be 2.5, and the conductivity of magnetite at these temperatures is metallic. Light irradiation also causes electron transfer, not only between ions occupying equivalent B-positions, but also between ions in different positions. In the first case, such transitions are called intervalent (IVCT — intervalence charge transfer), in the second case — intersublattice (ISCT — intersublattice charge transfer). The intensity of light absorption during such transitions is different for waves polarized along the right and left circles relative to the direction of the magnetic moment of the sample, which, in fact, is defined as magnetic circular dichroism. Along with such excitations, light irradiation causes transitions between the ground and excited states of individual ions split in the crystal field, the so-called transitions in the crystal field. The intensity of absorption during such transitions also depends on the sign of the circular polarization of the light wave. Thus, the range of transitions that contribute to the MCD of magnetite is quite extensive, and, as a result, the interpretation of the MCD spectra is not a simple task that attracts the attention of many researchers who use various approaches to solve it. Thus, in [36,37] the low-energy maximum in the spectra of the polar Kerr effect, as well as in the imaginary part of the off-diagonal component of the permittivity tensor ε''_{xy} obtained from its measurements, is associated with two overlapping transitions with charge transfer — near 2 eV with IVCT transition in the octahedral sublattice $[Fe^{2+}]_{t2g} \rightarrow [Fe^{3+}]_{eg}$, and in the area of 2.6 eV with an ISCT transition between the octahedral and tetrahedral sublattices $(Fe^{3+})_{t2} \rightarrow [Fe^{3+}]_{t2g}$. Similarly, the high-energy maximum is determined by the IVCT transition at 3.11 eV $[Fe^{2+}]_{t2g} \rightarrow (Fe^{3+})_e$ and the ISCT transition at 3.93 eV $(Fe^{3+})_{t2} \rightarrow [Fe^{3+}]_{eg}$.

In some works [34,20,38,39] first-principles calculations of the energy band structure of magnetite were performed and the spectra of MCD or the Kerr effect were analyzed in terms of charge transfer between exchange-split bands with different spin orientations. But even with this approach, the main contributions to the magnetooptical spectra in the spectral range under consideration are compared mainly with transitions similar to those described above. In [38], for example, the maximum of the Kerr effect at 2 eV is related

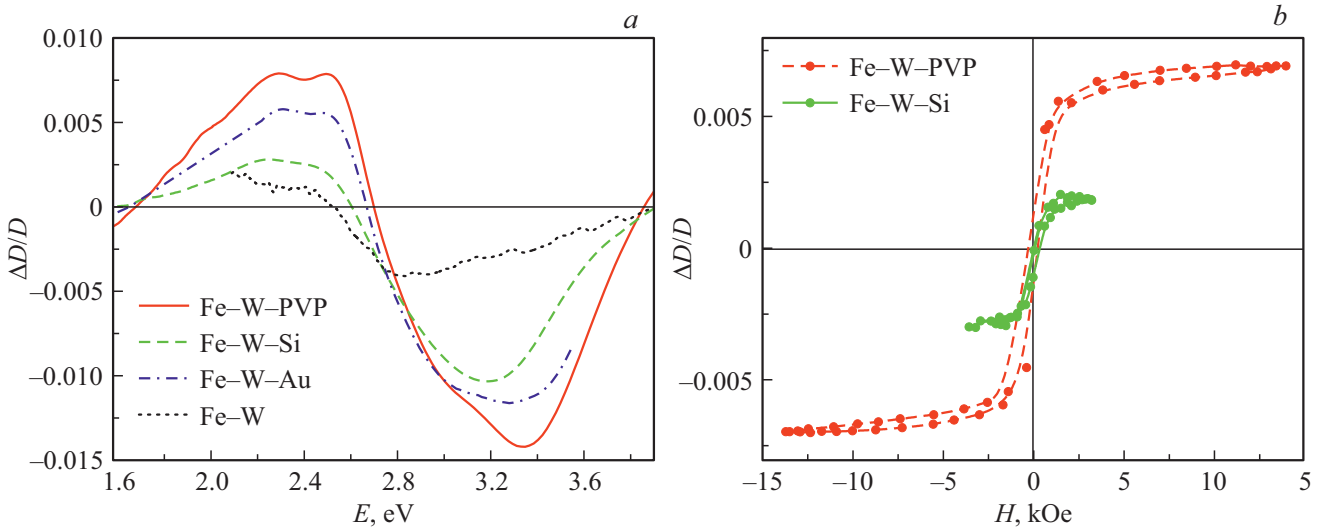

Figure 5. Spectral dependences of MCD for all samples (a) and field dependences of MCD for two samples (b). The spectral dependences were measured in a magnetic field 13 kOe, field dependences at a wavelength of 495 nm (~ 2.5 eV) at room temperature.

to the transition $Fe_B^{2+}(a_{1g\uparrow}) \rightarrow Fe_B^{3+}(e_{g\uparrow})$, and the peak between 3 and 4 eV is due to the $Fe_B^{3+}(e_{g\downarrow}) \rightarrow Fe_A^{3+}(e_{\downarrow}, t_{2\downarrow})$. In [38] it is calculated and experimentally shown how the spectrum of the Kerr effect is significantly rearranged when Fe^{3+} and/or Fe^{2+} ions are partially replaced by nonmagnetic Mg^{2+} or Al^{3+} ions. In particular, when substituting Mg^{2+}, which, in accordance with the valency, replaces Fe^{2+} ions in octahedral positions, the intensity of the low-energy maximum decreases, while the high-energy one, on the contrary, increases and it shifts to more high energies. Al^{3+} can replace Fe^{3+} in both types of positions, and this leads to broadening and some shift of both maxima to higher energies. Comparison of these data with the modification of the MCD spectra in the Fe-W-PVP and Fe-W-Au samples suggests that the synthesis of NPs using gold-hydrochloric acid and polyvinylpyrrolidone leads to deviations in the filling of positions with iron ions. Meanwhile, a greater deficit falls on Fe^{2+} in octahedra, which leads to a splitting of the maxima due to IVCT and ISCT transitions, and a shift of the maxima associated with IVCT to higher energies.

The field dependences of the MCD were measured for an energy of 2.5 eV. Since the MCD is linear in magnetization, the field dependences of the effect are proportional to the field dependences of the magnetization and allow to judge the type of magnetic ordering in the samples. Figure 5, b shows the field dependences of the MCD of the Fe-W-Si and Fe-W-PVP samples. The small and noisy signal of the spectral dependence of the MCD for the Fe-W sample is possibly due to the significant agglomeration of particles in the liquid and their precipitation, this fact did not allow measuring the field dependence in this sample, so it is not shown in the figure.

The presence of certain values of the residual effect and hysteresis at room temperature indicate a significant fraction of particles larger than the superparamagnetic limit for particles at room temperature.

4. Conclusion

The structural, optical, and magnetooptical properties of colloidal solutions of iron oxide nanoparticles obtained by laser ablation using various precursors have been studied. The TEM data revealed a strong influence of precursors on the nature of the size dispersion of nanoparticles and the degree of their agglomeration. If during ablation simply in distilled water there is an extremely wide scatter of sizes and strong agglomeration of particles, then for a number of Fe-W-Si, Fe-W-Au, Fe-W-PVP precursors, the distribution curve becomes increasingly narrow, and in the case of using PVP particles are the smallest, with a distribution maximum corresponding to the particle diameter ~ 7 nm, and there is no agglomeration. Meanwhile, the effects associated with the magnetization of nanoparticles (MCD) in samples coated with PVP are greater than in other samples. The spectral dependences of the MCD, while generally corresponding to the MCD spectra of magnetite, undergo some changes under the influence of various surface stabilizers on the magnetooptical response of nanoparticle solutions. These changes are presumably explained by deviations in the distribution of iron ions of different valences over the magnetic sublattices.

Acknowledgments

The authors would like to thank Dr. Phys.-Math. Sci., Professor I.S. Edelman for participating in the discussion of the study results and significant comments when writing the article. This study was supported by the Russian Foundation for Basic Research, grant No. 19-52-52002.

Conflict of interest

The authors declare that they have no conflict of interest.

References

[1] P.J. Camp. Modern Problems of Molecular Physics. Springer, Cham. (2018). P. 185.
[2] G. Barrera, P. Allia, P. Tiberto. J. Phys. D **54**, *31*, 315003 (2021).
[3] S. Chen, F. Fan, S. Chang, Y. Miao, M. Chen, J. Li, X. Wang, L. Lin. Opt. Express **22**, *6*, 6313 (2014).
[4] D.O. Zyatkov, V.B. Balashov, V.I. Yurchenko, E. Fakhrutdinova, V. Svetlichnyi, Z. Kochnev, A. Knyazkova, Yu. Kistenev, A.V. Borisov. Prog. Electromagn. Res. M **80**, 103 (2019).
[5] K.G. Gareev, V.V. Luchinin, E.N. Sevost'yanov, I.O. Testov, O.A. Testov. Tech. Phys. **64**, *6*, 893 (2019).
[6] K.G. Gareev. Magnetochemistry **6**, *2*, 24 (2020).
[7] D.V. Korolev, N.V. Evreinova, E.V. Zakharova, K.G. Gareev, E.B. Naumysheva, D.V. Postnov, V.N. Postnov, M.M. Galagudza. Russ. Chem. Bull. **68**, *5*, 1096 (2019).
[8] V. Nikiforov, E.Yu. Filinova. Magnetic Nanoparticles / Ed. S.P. Gubin. Weinheim, Wiley, (2009).
[9] A.G. Akopdzhanov, N.L. Shimanovskii, V.Yu. Naumenko, I.P. Suzdalev, V.K. Imshennik, Yu.V. Maksimov, S.V. Novichikhin. Him. Fizika **33**, *7*, 94 (2014) (in Russian).
[10] O.S. Kolovskaya, T.N. Zamay, G.S. Zamay, V. Babkin, E. Medvedeva, N. Neverova, A. Kirichenko, S.S. Zamay, I. Lapin, E. Morozov, A. Sokolov, A. Narodov, D.G. Fedorov, F.N. Tomilin, V. Zabluda, Yu. Alekhina, K.A. Lukyanenko, Yu. Glazyrin, V. Svetlichnyi, M.V. Berezovski, A.S. Kichkailo. Cancers **12**, *1*, 216 (2020).
[11] R. Lahoza, A. Naghilou, W. Kautek, O. Bomati-Miguel. Appl. Surf. Sci. **511**, 145438 (2020).
[12] V.A. Svetlichnyi, A.V. Shabalina, I.N. Lapin, D.A. Goncharova, D.A. Velikanov, A.E. Sokolov. Appl. Phys. A **123**, *12*, 763 (2017).
[13] V.A. Svetlichnyi, A.V. Shabalina, I.N. Lapin. Izv. vuzov. Fizika **59**, *12*, 30 (2016) (in Russian).
[14] V.A. Svetlichnyi, A.V. Shabalina, I.N. Lapin, D.A. Goncharova, T.S. Kharlamova, A.I. Stadnichenko. Appl. Surface Sci. **467**, 402 (2019).
[15] W. Wu, Q. He, Ch. Jiang. Nanoscale Res. Lett. **3**, 397 (2008).
[16] C. Vasilescu, M. Latikka, K.D. Knudsen, V.M. Garamus, V. Socoliuc, Rodica Turcu, Etelka Tombácz, Daniela Susan-Resiga, R.H.A. Ras, L. Vékás. Soft Matter **14**, *32*, 6648 (2018).
[17] E.N. Velichko, E.K. Nepomnyashchaya, K.G. Gareev, J. Martinez, M.C. Maicas. Appl. Sci.-basel **11**, *1*, 183 (2021).
[18] Y.G. Toropova, I.A. Zelinskaya, M.N. Gorshkova, D.S. Motorina, D.V. Korolev, F.S. Velikonivtsev, K.G. Gareev. J. Biomed. Mater. Res. A **1** (2021).
[19] Yu.E. Grebenkova, A.E. Sokolov, E.V. Eremin, I.S. Edelman, D.A. Marushchenko, V.I. Zaikovskiy, V.I. Chichkov, N.V. Andreev, Ya.M. Mukovsky. FTT **55**, *4*, 771 (2013) (in Russian).
[20] M.S. Alshammari, M.S. Alqahtani, H.B. Albargi, S.A. Alfihed, Y.A. Alshetwi, A.A. Alghihab, A.M. Alsamrah, N.M. Alshammari, M.A. Aldosari, A. Alyamani. Phys. Rev. B **90**, 144433 (2014).
[21] D. Ito, H. Ya. J. Magn. Magn. Mater. **500**, 166385 (2020).
[22] I. Edelman, O. Ivanova, R. Ivantsov, D. Velikanov, V. Zabluda, Y. Zubavichus, A. Veligzhanin, V. Zaikovskiy, S. Stepanov, A. Artemenko, J. Curély, J. Kliava. J. Appl. Phys. **112**, 084331 (2012).
[23] E. Tronc, C.Chanéac, J.P. Jolivet. J. Solid State Chem. **139**, 93 (1998).
[24] Y.El. Mendili, J.-F. Bardeau, N. Randrianantoandro, J.-M. Greneche, F. Grasset. Sci. Technol. Adv. Mater. **17**, *1*, 597 (2016).
[25] G. Campo, F. Pineider, V. Bonanni, M. Albino, A. Caneschi, César de Julián Fernández, C. Innocenti, C. Sangregorio. Chem. Mater. **27**, *2*, 466 (2015).
[26] R. Zboril, M. Mashlan, D. Petridis. Chem. Mater. **14**, 969 (2002).
[27] R.M. Cornell, U. Schwertmann. The iron oxides: structure, properties, reactions, occurrences and uses. John Wiley & Sons. (2003).
[28] V.A. Svetlichnyi, T.I. Izaak, I.N. Lapin, D.O. Martynova, O.A. Stonkus, A.I. Stadnichenko, A.I. Boronin. Adv. Powder Technol. **26**, *2*, 478 (2015).
[29] A.E. Sokolov, S.G. Ovchinnikov, V.N. Zabluda, A.M. Kalsin, Ya.V. Zubavichus. Pis'ma v ZhETF **2**, 104 (2013) (in Russian).
[30] A.V. Malakhovskii, U.V. Valiev, I.S. Edelman, A.E. Sokolov, I.Yu. Chesnokov, I.A. Gudim. Opt. Mater. **32**, 1017 (2010).
[31] Y. Vitta, V. Piscitelli, A. Fernandez, F. Gonzalez-Jimenez, J. Castillo. Chem. Phys. Lett. **512**, 96 (2011).
[32] Y. Liang, P. Liu, J. Xiao, H. Li, C. Wang, G. Yang. Sci. Rep. **3**, *3051*, 1 (2013).
[33] D.A. Petrov, C-R. Lin, R.D. Ivantsov, S.G. Ovchinnikov, S.M. Zharkov, G.Yu. Yurkin, D.A. Velikanov, Yu.V. Knyazev, M.S. Molokeev, Y.T. Tseng, E.S. Lin, I.S. Edelman, A.O. Baskakov, S.S. Starchikov, I.S. Lyubutin. Nanotechnology **31**, 395703 (2020).
[34] G.A. Gehring, M.S. Alshammari, D.S. Score, J.R. Neal, A. Mokhtari, A.M. Fox. J. Magn. Magn. Mater. **324**, 3422 (2012).
[35] J.R. Neal, A.J. Behan, A. Mokhtari, M.R. Ahmed, H.J. Blythe, A.M. Fox, G.A. Gehring. J. Magn. Magn. Mater. **310**, 246 (2007).
[36] W.F.J. Fontijn, P.J. van der Zaag, L.F. Feiner, R. Metselaar, M.A.C. Devillers. J. Appl. Phys. **85**, 5100 (1999).
[37] K.J. Kim, H.S. Lee, M.H. Lee, S. Ho Lee. J. Appl. Phys **91**, 9974 (2002).
[38] V.N. Antonov, B.N. Harmon, V.P. Antropov, A.Ya. Perlov, A.N. Yaresko. Phys. Rev. B. **64**, 134410 (2001).
[39] J. Chen, Hua-Shu Hsu, Ya-Huei Huang, Di-Jing Huang. Phys. Rev. B **98**, 085141 (2018).